Research Article | Vol. 26, No. 5 | 5 Mar 2018 | OPTICS EXPRESS 5368
Optics EXPRESS

Widely tunable, efficient 2 µm laser in monocrystalline Tm^{3+}:SrF_2

ALBERTO SOTTILE,[1,2,*] EUGENIO DAMIANO,[2,3] MARTINA RABE,[4] RAINER BERTRAM,[4] DETLEF KLIMM,[4] AND MAURO TONELLI[1,2]

[1]*NEST, Istituto Nanoscienze – CNR, Piazza S. Silvestro 12, Pisa, 56127, Italy*
[2]*Dipartimento di Fisica, Università di Pisa, Largo B. Pontecorvo 3, Pisa, 56127, Italy*
[3]*Dipartimento di Scienze Fisiche, della Terra e dell'Ambiente – Sez. di Fisica, Università di Siena, Via Roma 56, Siena, 53100, Italy*
[4]*IKZ – Leibniz-Institut für Kristallzüchtung, Max-Born-Str. 2, Berlin, 12489, Germany*
[*]*sottile@df.unipi.it*

Abstract: We report on the growth, spectroscopy, and laser operation of monocrystalline Tm^{3+}:SrF_2. Spectroscopic investigations confirmed the presence of broad absorption and emission bands caused by inequivalent doped sites, introduced by charge compensation effects which also caused the clusterization of doping ions in the lattice. We obtained continuous-wave laser emission at about 2 µm, with efficiencies comparable with other Tm-doped crystals. We also achieved an uninterrupted tuning range of 180 nm between 1.8 and 2 µm. This characterization indicates that SrF_2 enhances the cooperative mechanisms between Tm ions, helping to obtain remarkable laser performances at low doping concentrations.

OCIS codes: (140.3070) Infrared and far-infrared lasers; (140.3480) Lasers, diode-pumped; (140.3580) Lasers, solid-state; (140.3600) Lasers, tunable; (160.5690) Rare-earth-doped materials; (300.6280) Spectroscopy, fluorescence and luminescence.

References and links

1. K. Scholle, S. Lamrini, P. Koopmann, and P. Fuhrberg, "2 µm laser sources and their possible applications," in *Frontiers in Guided Wave Optics and Optoelectronics*, B. Pal, ed. (InTech, 2010), pp. 471–500.
2. R. Targ, B. C. Steakley, J. G. Hawley, L. L. Ames, P. Forney, D. Swanson, R. Stone, R. G. Otto, V. Zarifis, P. Brockman, R. S. Calloway, S. H. Klein, and P. A. Robinson, "Coherent lidar airborne wind sensor II: flight-test results at 2 and 10 µm," Appl. Opt. **35**, 7117–7127 (1996).
3. D. Theisen, V. Ott, H.-W. Bernd, V. Danicke, R. Keller, and R. Brinkmann, "Cw high-power IR laser at 2 µm for minimally invasive surgery," Proc. SPIE **5142**, 96–100 (2003).
4. V. Petrov, F. Guell, J. Massons, J. Gavalda, R. M. Sole, M. Aguilo, F. Diaz, and U. Griebner, "Efficient tunable laser operation of Tm:$KGd(WO_4)_2$ in the continuous-wave regime at room temperature," IEEE J. Quantum Electron. **40**, 1244–1251 (2004).
5. R. Moncorge, H. Manaa, M. Koselja, G. Boulon, C. Madej, C. Souriau, J., C. Borel, and C. Wyon, "Comparative optical study and 2 µm laser performance of the Tm^{3+} doped oxyde crystals: $Y_3Al_5O_{12}$, $YAlO_3$, $Gd_3Ga_5O_{12}$, Y_2SiO_5, $SrY_4(SiO_4)_3O$," J. Phys. IV France **04**,377–379 (1994).
6. F. Cornacchia, A. Toncelli, and M. Tonelli, "2-µm lasers with fluoride crystals: Research and development," Progr. Quant. Electron. **33**, 61–109 (2009).
7. K. van Dalfsen, S. Aravazhi, C. Grivas, S. M. García-Blanco, and M. Pollnau, "Thulium channel waveguide laser with 1.6 W of output power and 80% slope efficiency," Opt. Lett. **39**, 4380–4383 (2014).
8. W. B. Cho, A. Schmidt, J. H. Yim, S. Y. Choi, S. Lee, F. Rotermund, U. Griebner, G. Steinmeyer, V. Petrov, X. Mateos, M. C. Pujol, J. J. Carvajal, M. Aguiló, and F. Díaz, "Passive mode-locking of a Tm-doped bulk laser near 2 µm using a carbon nanotube saturable absorber," Opt. Express **17**, 11007–11012 (2009).
9. M. J. Cooper and K. D. Rouse, "A neutron diffraction study of SrF_2 and CaF_2," Acta Cryst. A **27**, 622–628 (1971).
10. J. Boudeile, J. Didierjean, P. Camy, J. L. Doualan, A. Benayad, V. Ménard, R. Moncorgé, F. Druon, F. Balembois, and P. Georges, "Thermal behaviour of ytterbium-doped fluorite crystals under high power pumping," Opt. Express **16**, 10098–10109 (2008).
11. U. Ranon and A. Yaniv, "Charge compensation by interstitial F^- ions in rare-earth-doped SrF_2 and BaF_2," Phys. Lett. **9**, 17–19 (1964).
12. S. A. Payne, J. A. Caird, L. L. Chase, L. K. Smith, N. D. Nielsen, and W. F. Krupke, "Spectroscopy and gain measurements of Nd^{3+} in SrF_2 and other fluorite-structure hosts," J. Opt. Soc. Am. B **8**, 726–740 (1991).

#313810 https://doi.org/10.1364/OE.26.005368
Journal © 2018 Received 21 Nov 2017; revised 17 Jan 2018; accepted 24 Jan 2018; published 22 Feb 2018

Optics EXPRESS

13. R. Gaumé, B. Viana, D. Vivien, J.-P. Roger, and D. Fournier, "A simple model for the prediction of thermal conductivity in pure and doped insulating crystals," Appl. Phys. Lett. **83**, 1355–1357 (2003).
14. T. P. J. Han, G. D. Jones, and R. W. G. Syme, "Site-selective spectroscopy of Nd^{3+} centers in CaF_2:Nd^{3+} and SrF_2:Nd^{3+}," Phys. Rev. B **47**, 14706–14723 (1993).
15. O. K. Alimov, M. E. Doroshenko, V. A. Konyushkin, A. G. Papashvili, and V. V. Osiko, "Selective laser spectroscopy of SrF_2 crystal doped with Pr^{3+} ions," Quantum Electron. **46**, 68 (2016).
16. P. Camy, J. L. Doualan, S. Renard, A. Braud, V. Ménard, and R. Moncorgé, "Tm^{3+}:CaF_2 for 1.9 μm laser operation," Opt. Commun. **236**, 395–402 (2004).
17. F. Druon, S. Ricaud, D. N. Papadopoulos, A. Pellegrina, P. Camy, J. L. Doualan, R. Moncorgé, A. Courjaud, E. Mottay, and P. Georges, "On Yb:CaF_2 and Yb:SrF_2: review of spectroscopic and thermal properties and their impact on femtosecond and high power laser performance [Invited]," Opt. Mater. Express **1**, 489–502 (2011).
18. T. T. Basiev, M. E. Doroshenko, V. A. Konyushkin, and V. V. Osiko, "SrF_2:Nd^{3+} laser fluoride ceramics," Opt. Lett. **35**, 4009–4011 (2010).
19. T. T. Basiev, Y. V. Orlovskii, M. V. Polyachenkova, P. P. Fedorov, S. V. Kuznetsov, V. A. Konyushkin, V. V. Osiko, O. K. Alimov, and A. Y. Dergachev, "Continuously tunable cw lasing near 2.75 μm in diode-pumped Er^{3+}:SrF_2 and Er^{3+}:CaF_2 crystals," Quantum Electron. **36**, 591 (2006).
20. M. E. Doroshenko, V. A. Konyushkin, N. A. Nakladov, P. P. Fedorov, V. V. Osiko, K. A. Martynova, H. Jelinkova, and J. Sulc, "Spectroscopic and laser properties of Tm^{3+} ions in fluoride crystals and ceramics," in *2014 International Conference Laser Optics* (ICLO, 2014), p. 1.
21. H. H. Li, "Refractive index of alkaline earth halides and its wavelength and temperature derivatives," J. Phys. Chem. Ref. Data **9**, 161–290 (1980).
22. P. Dorenbos and H. W. den Hartog, "Space charges and dipoles in rare-earth-doped SrF_2," Phys. Rev. B **31**, 3932–3938 (1985).
23. S. Renard, P. Camy, A. Braud, J. L. Doualan, and R. Moncorgé, "CaF_2 doped with Tm^{3+}: A cluster model," J. Alloy. Compd. **451**, 71–73 (2008).
24. D. Maier, R. Bertram, D. Klimm, and R. Fornari, "Influence of the atmosphere on the growth of $LiYF_4$ single crystal fibers by the micro-pulling-down method," Cryst. Res. Technol. **44**, 137–140 (2009).
25. B. P. Sobolev and K. B. Seiranian, "Phase diagrams of systems SrF_2–(Y,Ln)F_3. II. Fusibility of systems and thermal behavior of phases," J. Solid State Chem. **39**, 337–344 (1981).
26. A. S. Jordan, "A theory of regular associated solutions applied to the liquidus curves of the Zn-Te and Cd-Te systems," Met. Trans. **1**, 239–249 (1970).
27. P. Rudolph, "Defect formation during crystal growth from the melt," in *Springer Handbook of Crystal Growth*, G. Dhanaraj, K. Byrappa, V. Prasad, and M. Dudley, eds. (Springer, Berlin, Heidelberg, 2010), pp. 159–201.
28. J. A. Burton, E. D. Kolb, W. P. Slichter, and J. D. Struthers, "Distribution of Solute in Crystals Grown from the Melt. Part II. Experimental," J. Chem. Phys. **21**, 1991–1996 (1953).
29. D. Parisi, S. Veronesi, A. Volpi, M. Gemmi, M. Tonelli, A. Cassanho, and H. P. Jenssen, "Spectroscopy and laser test emission in Tm^{3+}:$BaYLuF_8$ single crystal," J. Phys. D: Appl. Phys.. **47**, 025101 (2014).
30. A. Braud, S. Girard, J. L. Doualan, M. Thuau, R. Moncorgé, and A. M. Tkachuk, "Energy-transfer processes in Yb:Tm-doped KY_3F_{10}, $LiYF_4$, and BaY_2F_8 for laser operation at 1.5 and 2.3 μm," Phys. Rev. B **61**, 5280–5292 (2000).
31. G. Huber, W. W. Krühler, W. Bludau, and H. G. Danielmeyer, "Anisotropy in the laser performance of NdP_5O_{14}," J. Appl. Phys. **46**, 3580–3584 (1975).
32. H. Kopfermann and R. Ladenburg, "Experimental Proof of 'Negative Dispersion'," Nature. **122**, 438–439 (1928).
33. S. Payne, L. Chase, L. K. Smith, W. L. Kway, and W. F. Krupke, "Infrared cross-section measurements for crystals doped with Er^{3+}, Tm^{3+}, and Ho^{3+}," IEEE J. Quantum Electron.. **28**, 2619–2630 (1992).
34. F. Cornacchia, D. Parisi, and M. Tonelli, "Spectroscopy and Diode-Pumped Laser Experiments of $LiLuF_4$:Tm^{3+} Crystals," IEEE J. Quantum Electron.. **44**, 1076–1082 (2008).
35. S. Veronesi, Z. Jia, D. Parisi, E. Damiano, W. Mu, Y. Yin, M. Tonelli, and X. Tao, "Spectroscopy and diode pumped laser emission in $(Lu_xGd_{(1-x)})_3Ga_5O_{12}$:$Tm^{3+}$ single crystal," J. Phys. D: Appl. Phys.. **48**, 385302 (2015).
36. P. Loiko, X. Mateos, S. Y. Choi, F. Rotermund, J. M. Serres, M. Aguiló, F. Díaz, K. Yumashev, U. Griebner, and V. Petrov, "Vibronic thulium laser at 2131 nm Q-switched by single-walled carbon nanotubes," J. Opt. Soc. Am. B **33**, D19–D27 (2016).
37. B. R. Judd, "Optical Absorption Intensities of Rare-Earth Ions," Phys. Rev. **127**, 750 (1962).
38. G. S. Ofelt, "Intensities of Crystal Spectra of Rare–Earth Ions," J. Chem. Phys. **37**, 511 (1962).
39. B. M. Walsh, N. P. Barnes, and B. Di Bartolo, "Branching ratios, cross sections, and radiative lifetimes of rare earth ions in solids: Application to Tm^{3+} and Ho^{3+} ions in $LiYF_4$," J. Appl. Phys. **83**, 2772–2787 (1998).
40. C. M. Dodson and R. Zia, "Magnetic dipole and electric quadrupole transitions in the trivalent lanthanide series: Calculated emission rates and oscillator strengths," Phys. Rev. B **86**, 125102 (2012).
41. F. Cornacchia, A. Di Lieto, and M. Tonelli, "$LiGdF_4$:Tm^{3+} spectroscopy and diode-pumped laser experiments," Appl. Phys. B **96**, 363–368 (2009).
42. R. Lisiecki, P. Solarz, G. Dominiak-Dzik, W. Ryba-Romanowski, M. Sobczyk, P. Černý, J. Šulc, H. Jelínková, Y. Urata, and M. Higuchi, "Comparative optical study of thulium-doped YVO_4, $GdVO_4$, and $LuVO_4$ single crystals," Phys. Rev. B **74**, 035103 (2006).

Optics EXPRESS

43. L. B. Shaw, R. S. F. Chang, and N. Djeu, "Measurement of up-conversion energy-transfer probabilities in Ho:$Y_3Al_5O_{12}$ and Tm:$Y_3Al_5O_{12}$," Phys. Rev. B **50**, 6609–6619 (1994).
44. G. Galzerano, F. Cornacchia, D. Parisi, A. Toncelli, M. Tonelli, and P. Laporta, "Widely tunable 1.94-μm Tm:BaY_2F_8 laser," Opt. Lett. **30**, 854–856 (2005).
45. P. Koopmann, S. Lamrini, K. Scholle, P. Fuhrberg, K. Petermann, and G. Huber, "Efficient diode-pumped laser operation of Tm:Lu_2O_3 around 2 μm," Opt. Lett. **36**, 948–950 (2011).
46. Y. Wang, J. Lan, Z. Zhou, X. Guan, B. Xu, H. Xu, Z. Cai, Y. Wang, and C. Tu, "Continuous-wave laser operation of diode-pumped Tm-doped $Gd_3Ga_5O_{12}$ crystal," Opt. Mater. **66**, 185–188 (2017).
47. J. M. Cano-Torres, M. D. Serrano, C. Zaldo, M. Rico, X. Mateos, J. Liu, U. Griebner, V. Petrov, F. J. Valle, M. Galán, and G. Viera, "Broadly tunable laser operation near 2 μm in a locally disordered crystal of Tm^{3+}-doped $NaGd(WO_4)_2$," J. Opt. Soc. Am. B **23**, 2494–2502 (2006).
48. X. Mateos, J. Liu, H. Zhang, J. Wang, M. Jiang, U. Griebner, and V. Petrov, "Continuous-wave and tunable laser operation of Tm:$LuVO_4$ near 1.9 μm under Ti:sapphire and diode laser pumping," Phys. Stat. Sol. **203**, R19–R21 (2006).
49. N. Coluccelli, G. Galzerano, P. Laporta, F. Cornacchia, D. Parisi, and M. Tonelli, "Tm-doped $LiLuF_4$ crystal for efficient laser action in the wavelength range from 1.82 to 2.06 μm," Opt. Lett. **32**, 2040–2042 (2007).
50. P. Koopmann, R. Peters, K. Petermann, and G. Huber, "Crystal growth, spectroscopy, and highly efficient laser operation of thulium-doped Lu_2O_3 around 2 μm," Appl. Phys. B **102**, 19–24 (2011).

1. Introduction

Over the last decade, many solid-state laser sources have been developed in the wavelength region that goes from 1.8 to 2 μm. Reasons for this scientific and industrial interest lie in the variety of applications that these sources enable, including gas detection, frequency metrology, nonlinear oscillator pumping, and high-resolution spectroscopy, but also in the strong absorption band of liquid water in this wavelength range. This absorption band makes these sources eye-safe, allowing their employment in long-range LIDAR devices or in biomedical equipment with controlled penetration depths [1–3].

Thulium-based solid-state lasers have already shown broadly tunable laser emissions in this range, using multiple host materials [4–6]. Trivalent Tm ions can be efficiently pumped using inexpensive and high-power AlGaAs-based laser diodes, emitting at about 0.8 μm. Moreover, Tm presents a cross-relaxation cooperative mechanism that allows to excite two ions in the upper laser level using a single pump photon, decreasing the quantum defect of the laser, increasing the source efficiency, and reducing the parasitic heat load on the host material [7].

Lasers based on Tm ions have been developed in multiple geometries and classes of materials, including glasses, ceramics, single crystals, and active optical fibers. Monocrystalline materials present some advantages with respect to those other systems, such as improved thermal conductivity and larger power scalability. In addition, Tm-doped single crystals have been successfully employed as active media for Q-switching and mode-locking pulsed lasers, typically with better performances in comparison with other classes of materials and fiber lasers [8].

Among all the monocrystalline hosts available, fluorite-structure crystals such as calcium fluoride (CaF_2) and strontium fluoride (SrF_2) show multiple appealing properties for designing laser sources. Firstly, they have a simple cubic structure with well known parameters, which allow to fabricate, study, and handle samples of these materials without taking care of their crystallographic orientation [9]. Secondly, they have good thermal and mechanical properties, especially in comparison with other, more complex, fluorides [10].

In addition to that, the formation of dopant clusters in these materials has been reported so far with several rare earth ions, leading to an increase of the cooperative processes. These clusters are caused by charge compensation effects, required to accomodate a trivalent ion in the divalent strontium sites [11]. This feature should be particularly beneficial for Tm-based sources because they rely on cross-relaxation between interacting ions to increase their efficiency [12]. Clusters should allow to obtain the same cross-relaxation rate at lower doping concentrations, reducing any stresses that may affect the host, hence improving the thermo-mechanical properties of the doped crystal [13]. Furthermore, despite their cubic lattice, fluorite-like crystals still have broad

Optics EXPRESS

absorption and emission spectra, because the doped sites in the lattice become inequivalent due to the same compensation effects that caused clustering [14, 15]. Broad emission spectra make these crystals particularly appealing for mode-locked lasers with ultrashort pulses, which are of interest for many of the potential applications listed above.

While both CaF_2 and SrF_2 have been historically considered as promising laser hosts, these effects were demonstrated only in the former so far when doped with thulium ions. Indeed, lasers based on Tm:CaF_2 have shown efficiencies comparable with other hosts with much lower Tm concentrations [16]. On the other hand, the laser performance of rare-earth-doped SrF_2 have been inferior so far, as only a few laser results have been reported in this host, mostly in ceramics or other composite materials [17–20].

In this paper, we report, to the best of our knowledge, on the first laser operation of monocrystalline Tm-doped SrF_2 (Tm:SrF_2). Properties of the grown crystal and of its dopant distribution were investigated with elemental analyses. A full spectroscopic characterization was performed on the material in the spectral regions of interest. We tested the laser performance of this crystal using two pumping schemes, and we achieved continuous-wave laser operation at 2 μm, with slope efficiencies comparable with other Tm-doped crystals. Furthermore, we investigated the wavelength tunability of this source, obtained an uninterrupted tuning range of 180 nm, between 1.8 and 2 μm, on par with other crystalline hosts.

2. Crystal properties and growth details

For this characterization, a single crystal of SrF_2 doped with the 5.2 mol.% of Tm^{3+} ions was grown in the laboratories of the *Leibniz-Institut für Kristallzüchtung (IKZ)* in Berlin, Germany. We chose a lower doping concentration than those usually employed for Tm-doped fluoride crystals (typically between 8 mol.% and 16 mol.% [6]) because we wanted to verify the effects of ion clusterization on the laser performances. Measurements of the dopant distribution inside the grown Tm:SrF_2 crystals were also performed at the *IKZ*.

2.1. Material properties

Crystalline SrF_2 has the cubic structure of simple fluorides, with the space group $Fm\bar{3}m$ and lattice constant $a = 0.578$ nm [15]. Its transparency window extends from 0.12 to 20 μm, making it suitable for laser experiments at various wavelengths. It has a thermal conductivity of about $8\,W/(m \cdot K)$ and a refractive index of 1.43 at 2 μm [21]. SrF_2 has also a low phonon energy, about 400 cm^{-1} and a low Stark splitting, similar to other fluorides [17]. These properties normally lead to sharp, narrow absorption and emission bands, centered at the electronic levels of the embedded ion, especially in the case of rare-earth doping.

However, since the strontium is in a divalent oxidation state in SrF_2, its substitution with trivalent rare-earth ions introduces a charge mismatch in the lattice, differentiating the doping sites and causing inhomogeneous broadening of the optical transitions [14]. This effect leads to broad spectral bands at room temperature, which are particularly appealing for pulsed lasers with ultrashort pulses. In addition, clusters of doping ions tend to form, increasing local dopant density and the interaction between neighbor ions [22].

Trivalent Tm ions present a cross-relaxation cooperative process that involves two close ions, initially in the excited $^3H_4$ state and in the fundamental $^3H_6$ level, respectively. The excited ion interacts with the other and donates part of its energy, enough to raise the energy of the second ion and bring it to an intermediate state, the $^3F_4$. As a result, the energy of the excited ion decreases and so also this ion reaches the same intermediate level. At the end of this cooperative process, the two ions populate the $^3F_4$ level [6]. This mechanism is widely used to achieve population inversion for the $^3F_4 \rightarrow {}^3H_6$ transition in Tm-based lasers, and is also exploited in this work. Such cooperative processes are likely to be enhanced in the clusters of doping ions that tend to form in SrF_2, and indeed this enhancement has been reported in Er:SrF_2 and Tm:CaF_2 and

Optics EXPRESS

attributed to the formation of clusters [19, 23].

2.2. Growth parameters

Crystal growth was performed with the Czochralski technique, using a graphite crucible with a passive graphite afterheater. To obtain the desired TmF_3 concentration of about 5 mol.% in the crystal, we prepared a starting mixture with 5.43 mol.% by mixing high-purity crystalline SrF_2 (Korth Kristalle, Germany) with TmF_3 powders (Meldform, 99.99% purity), treated before with fluorine at 200 °C for 20 hours to further remove any traces of oxides and moisture. Before starting the growth process, the furnace chamber was evacuated and slightly heated while under vacuum (up to a few hundred °C) to remove adsorbed moisture. Then, the chamber was filled to 1 bar with a mixture of 5 vol.% CF_4 gas in N_2. A flux of the same atmosphere was maintained during the whole growth process, in order to grow an inclusion-free crystal [24]. The growing boule was pulled at 0.6 mm/h along the ⟨111⟩ crystallographic direction and rotated at a rate between 10 and 22 min^{-1}. The finished boule was 37 mm long, with a diameter between 16 and 18 mm, and a weight of 37.5 g. The whole crystal was optically clear, but showed some cracks and even polycrystalline regions.

2.3. Estimation of dopant segregation in Tm:SrF_2

Figure 1 shows the phase diagram of the SrF_2–TmF_3 pseudobinary system, in the region of interest for this work [25]. From this plot, it is clear that thulium is depleted in the solid with respect to the liquid during a crystal growth from the melt. This causes a variation in the doping level of the crystal along the growth direction, called dopant segregation. Let c_s and c_l be the concentrations of TmF_3 in the solid or liquid phase, respectively. Their relation is described by the equilibrium distribution coefficient $k = c_s/c_l$. Often k is assumed to be constant, an approximation that actually holds if liquidus and solidus are linear. A better approximation can be obtained, at least for small doping concentrations, if both phase boundaries are fitted with parabolas [26, 27].

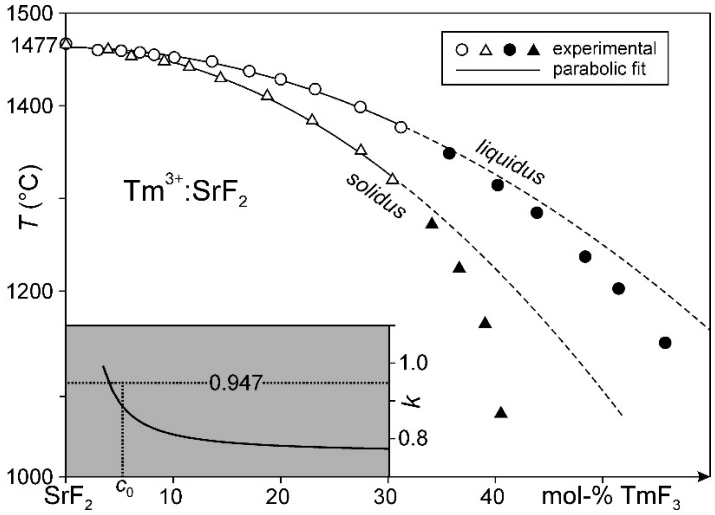

Fig. 1. Strontium-rich part of the SrF_2–TmF_3 phase diagram, with quadratic fits of liquidus and solidus lines up to 30 mol.% of TmF_3. The experimental points were taken from [25]. Inset: calculated equilibrium distribution coefficient as a function of the concentration in the liquid. c_0 is the initial concentration chosen for this crystal growth.

Optics EXPRESS

Using the data reported in Fig. 1, this fit was possible for TmF_3 concentrations up to 30 mol.%. From these parabolic fits, we calculated the distribution coefficient $k(c)$, plotted in the inset of Fig. 1. Experimental uncertainties and fitting errors do not allow the calculation of k for smaller values of c, but for larger concentrations k starts near unity and then drops smoothly to $k \approx 0.77$. According to this calculation, the distribution coefficient should be equal to 0.89 at the initial doping concentration c_0 chosen for our Tm:SrF_2 crystal. It should be noted that this distribution coefficient is valid under equilibrium conditions, whereas under kinetic crystallization conditions the effective distribution coefficient k_{eff} can shift further towards unity [28].

To estimate the effective segregation inside our crystal, we measured the chemical concentration of TmF_3 in two pieces, taken from the head and from the tail of the boule. This analysis was conducted using an *IRIS Intrepid HR Duo* (Thermo Elemental, U.S.A.) ICP–OES spectrometer. The concentration of thulium fluoride was estimated to be 5.14 mol.% in the head and 5.21 mol.% in the tail, which crystallized later. Thus, the average concentration of Tm ions inside the crystal was 1.07×10^{21} ions/cm^3. The variation of concentration of Tm^{3+} along the growth direction in our boule can be described by $k_{\text{eff}} = 0.947$. This value is shown as a dashed line in Fig. 1, neglecting its dependency from the concentration. This *a posteriori* estimation of k_{eff} is close to the calculated value of $k(c_0) = 0.89$.

3. Spectroscopic characterization

To study the spectral properties of this Tm:SrF_2 crystal, we prepared a parallelepiped sample for spectroscopic measurements, polished on two facets to improve their optical quality. We then measured its absorption and fluorescence spectra, in the wavelength ranges of interest for pumping and emission. We also measured the decay time of the upper laser level of thulium. These data were employed to calculate the laser gain curves for this material. We also estimated the cross-relaxation rate in our crystal using an indirect analysis performed on the available data.

3.1. Absorption spectrum

We employed an integrated spectrophotometer *Cary 5000* (Agilent, U.S.A.) to perform absorption measurements on the sample. We acquired the spectrum from 750 to 850 nm, in the wavelength range suitable for pumping the $^3H_4$ manifold of Tm^{3+} ions, with a resolution of 0.3 nm. We also measured the absorption band of the upper laser level $^3F_4$, which goes from 1.5 to 2 μm, with a resolution of 1.5 nm. Since this band is resonant with the emission from the upper laser level, we used these data to evaluate the effects of reabsorption on the laser performance. A complete absorption spectrum was also acquired for a subsequent Judd–Ofelt analysis, extending from 300

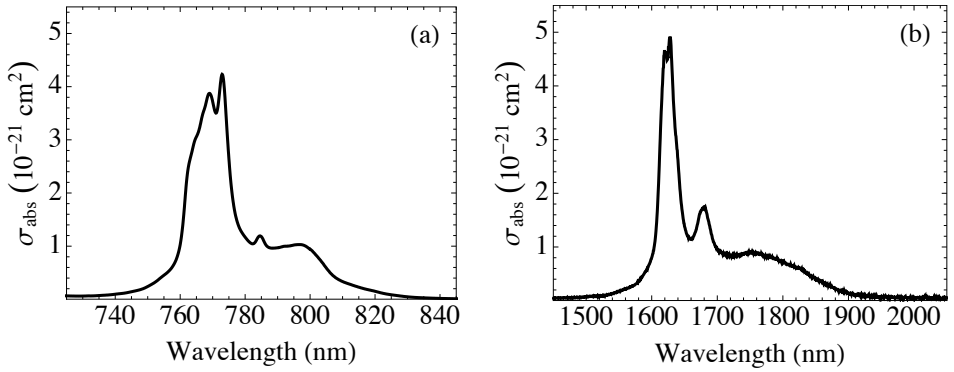

Fig. 2. Ground-state absorption cross-section of monocrystalline Tm:SrF_2 for the transitions that reach the $^3H_4$ manifold (a) and the $^3F_4$ manifold (b).

Optics EXPRESS

to 850 nm, with a resolution of 0.3 nm, and from 850 to 2100 nm, with a resolution of 1.5 nm. All these measurements were performed with the sample at room temperature.

From the absorption coefficient, we calculated the absorption cross-section σ_{abs} of Tm:SrF_2, using the concentration data reported in the previous paragraph. Results of these measurements are shown in Fig. 2. From both plots, it can be seen that the transition peaks are surrounded by a broad background, caused by the charge mismatch mentioned before. The wide pedestal near 790 nm reported in Fig. 2(a) extends for about 40 nm and makes this crystal particularly appealing for pumping it with inexpensive AlGaAs-based laser diodes.

3.2. Static and dynamic fluorescence measurements

Fluorescence spectra were acquired in the infrared region between 1.5 and 2.2 μm for the transition of trivalent thulium ions between the upper laser level $^3F_4$ and the fundamental state $^3H_6$. For this measurement, we employed a custom-made continuous-wave Ti:Sa tunable laser as pump source, tuned to emit at 772 nm to maximize the absorption efficiency. The sample of Tm:SrF_2 was mounted in a L-shaped holder that minimizes the path traveled by the fluorescence inside the crystal, with the goal to mitigate reabsorption effects.

The fluorescence was chopped, sent through a monochromator with a 300 g/mm diffraction grating, and sampled using an InSb photodiode. The signal of the photodiode was cleaned and amplified by a lock-in amplifier. This equipment allowed to acquire the infrared emission spectrum of the crystal with a resolution of 5 nm. This spectrum was then corrected for the spectral response of the detection system, determined using a black-body lamp at 3000 K.

We investigated possible site-selective effects in Tm:SrF_2 by measuring this fluorescence spectrum at various pump wavelengths. We tuned the pump laser wavelength between 763 and 790 nm and we did not observe significant differences in the recorded spectra, excluding the appearance of these effects at room temperature.

With the same equipment, we measured the decay time of the upper laser level $^3F_4$. We employed a custom-made pulsed Ti:Sa tunable laser as pump source, with pulse duration of 30 ns and repetition rate of 10 Hz, tuned to emit at 772 nm. A digital oscilloscope was synchronized with the pulses and used to acquire the decay curve. We observed a single-exponential profile,

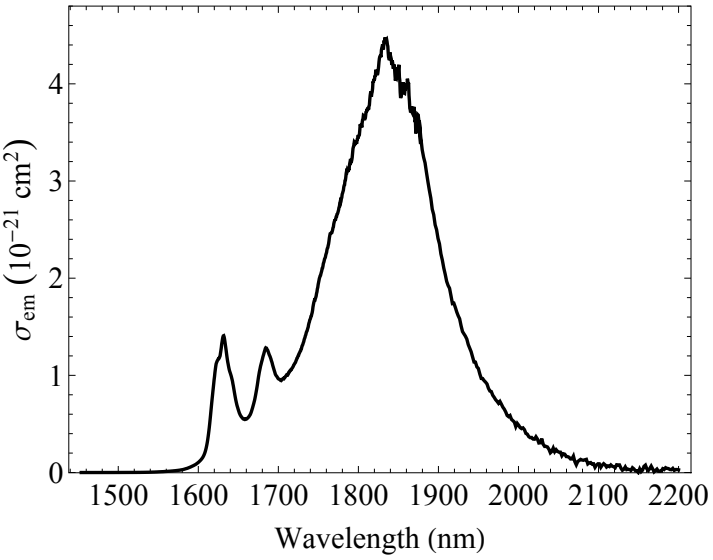

Fig. 3. Emission cross-section of the $^3F_4$ manifold in monocrystalline Tm:SrF_2.

Optics EXPRESS

and calculated a decay time of (8.8 ± 0.1) ms, similar to existing reports on other Tm-doped fluoride crystals [29]. We also investigated the decay curve of the $^3H_4$ level, and we observed a non-exponential profile with an effective lifetime of 3 µs, short enough to confirm the presence of the cross-relaxation process described before [30].

We evaluated the stimulated emission cross-section σ_{SE} of the $^3F_4$ manifold in Tm:SrF_2, using the fluorescence spectrum and the decay data, via the Füchtbauer–Ladenburg relation [31, 32]. To further reduce the influence of reabsorption, we also evaluated the emission-cross section with the reciprocity method [33], using the absorption spectrum reported in Fig. 2(b), and scaling the resulting curve to the data obtained from the fluorescence spectrum.

Figure 3 shows the emission cross-section of this material in the 2 µm region. For the long wavelength region (above 1.9 µm), we picked the estimation given by the Füchtbauer–Ladenburg relation, whereas the short wavelength region was evaluated with the reciprocity method. Peak values of the emission cross-section are on par with other thulium-doped crystals [34, 35]. In addition, a broadening of the emission band is evident, introduced by the charge compensation effects mentioned earlier.

We also estimated the laser gain cross-section $\sigma_g = \beta\sigma_{SE} - (1 - \beta)\sigma_{abs}$ of our sample of Tm:SrF_2, where the parameter β is the ratio between the population density of the upper laser level and density of embedded thulium ions. We used the absorption and emission cross-section data, measured as described before. Figure 4 shows the gain curves for several values of the β factor. It can be seen that the gain exhibits a long tail that extends above 2 µm. Gain cross-section peak values have the same order of magnitude than other Tm-based solid-state lasers [36].

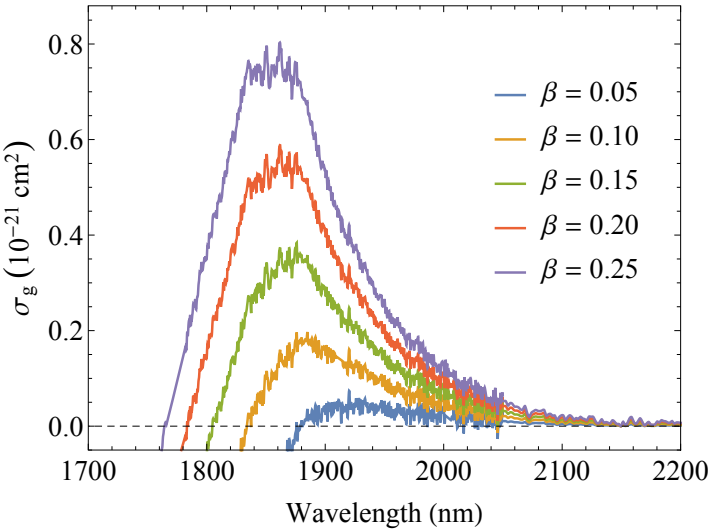

Fig. 4. Laser gain cross-section for the $^3F_4$ manifold in monocrystalline Tm:SrF_2.

3.3. *Estimation of the cross-relaxation rate*

Quantifying the enhancement of the cross-relaxation caused by clustering would require to measure the cross-relaxation rate W_{CR} in this crystal. This rate can be expressed as the difference of the reciprocals of the actual lifetime of the quenched level, the $^3H_4$, minus the radiative lifetime of the same level, defined as the decay time in absence of any non-radiative processes [23]. A direct measurement of this radiative lifetime necessitates the growth of a sample with a very low doping concentration, which was not available at the time of this work.

We estimated indirectly this quantity using the standard Judd–Ofelt (J–O) theory on data

Optics EXPRESS

from a multi-band absorption spectrum of our crystal [37, 38]. All the parameters needed for the calculations were taken from [39, 40]. For our Tm:SrF_2 crystal, we determined the J–O intensity parameters as $\Omega_2 = 1.298$, $\Omega_4 = 3.519$, and $\Omega_6 = 2.444$ $\left[10^{-20}\ \mathrm{cm}^2\right]$. The radiative lifetime of the $^3H_4$ was estimated to be 1.6 ms. Comparing this value with the actual lifetime of the same level, measured as described before, the cross-relaxation rate was calculated as $W_{CR} \approx 3 \times 10^5\ \mathrm{s}^{-1}$. In comparison with other Tm-doped crystals with approximately the same concentration of ions, this value is higher than in several materials [34, 41, 42], suggesting that the cross-relaxation is indeed enhanced in Tm:SrF_2. It should be noted, though, that there are other crystals in which this parameter is still higher [43].

4. Laser experiments

We performed a characterization of the laser performance on monocrystalline Tm:SrF_2 by testing its free-running continuous-wave emission in a two-mirror resonator, pumping the crystal with two different sources. We also evaluated the wavelength tunability of this solid-state laser in a three-mirror cavity.

4.1. Experimental setup

We prepared a parallelepiped-shaped sample of monocrystalline Tm:SrF_2 specifically for laser tests, 8.8 mm long and with a transverse cross-section of $8.6 \times 6.1\ \mathrm{mm}^2$. The two smallest facets were polished to reduce any parasitic scattering and enhance their optical quality. No coating was applied on these facets. During the experiments, this crystal was mounted in a copper holder and refrigerated with recirculating water at 18° C.

For the free-running laser experiments, we used a hemispherical resonant cavity, made of a plane input mirror and a plane-concave output mirror with a radius of curvature of 100 mm. Both the mirrors were highly-reflective coated from 1900 to 2100 nm, and the output coupler had a transmittance of 0.3% at about 2 µm. The input mirror had a transmittance greater than 97% between 770 and 800 nm, to allow transmission of the pump laser beam, which was focused in the Tm:SrF_2 sample by using a 40 mm achromatic lens.

We tested the laser performance of this crystal using two pump sources. We started our investigation using the custom-made continuous-wave Ti:Sa tunable laser employed during the measurements of the fluorescence spectra. This laser was tuned to emit at 787 nm, with an output power of 1.4 W, and had a quasi-diffraction-limited output beam. To investigate an alternative pumping scheme, we employed a fiber-coupled diode laser, capable of emitting 3.3 W at 787 nm, but with a much lower spectral quality and spatial coherence than the former source. For both

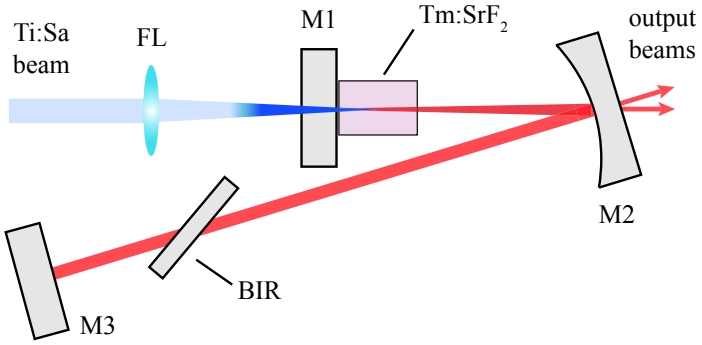

Fig. 5. Layout of the resonator employed during the tunability experiments. All the labels are defined in text.

Optics EXPRESS

pumping schemes, we measured the single-pass absorption efficiency of the Tm:SrF_2 sample via transmission measurements, obtaining about 51% under Ti:Sa excitation and about 55% under laser diode excitation.

For the wavelength tunability experiments, we employed a three-mirror V-shaped resonant cavity, made using the two mirrors described earlier (M1 and M2), plus a third plane mirror (M3), also highly-reflective coated between 1900 and 2100 nm. In this case, the curved mirror M2 was placed at about 50 mm from the input mirror M1, tilted by an angle of about 20°, creating an almost-collimated beam in the second arm of the resonator. We inserted a 2-mm-thick quartz birefringent plate (BIR) in this arm, placed at Brewster's angle, to perform the wavelength selection. Because the cavity was folded on the output mirror, this resonator had two output beams escaping from the curved mirror M2, effectively causing a total transmittance of 0.6% at about 2 μm. Figure 5 shows a scheme of this setup. During these tunability experiments, we used only the Ti:Sa laser described before as pump source, tuned to emit at 777 nm, focused in the crystal using a 40 mm achromatic lens (FL). In these conditions, the single-pass absorption efficiency of the Tm:SrF_2 crystal was about 65%.

In all the experiments, a coated silicon filter was placed behind the output mirror to remove any residual pump power. We measured the input and output powers using a thermal power meter. To acquire the spectrum of the output laser, we sent a fraction of the output beam to the same equipment employed during the fluorescence measurements. Laser spectra were sampled with a resolution of 0.4 nm. This higher resolution was possible because of the much higher brightness of this source with respect to the fluorescence light.

4.2. *Free-running laser results*

In the free-running experiments, we obtained continuous-wave laser emission from the Tm:SrF_2 crystal in study in the 2 μm region. By pumping the crystal with our Ti:Sa laser, we obtained a slope efficiency of 50% with respect to the absorbed pump power, a maximum output power of 240 mW with an absorbed pump power of 0.6 W, and a threshold absorbed power of 65 mW. In this configuration, the output laser had an average wavelength of about 2015 nm. Data obtained in this pumping scheme are reported in Fig. 6(a).

We then proceeded by switching the pump source and employing the laser diode described before. In this pumping scheme, we obtained a slope efficiency of 43% with respect to the absorbed pump power, a maximum output power of 530 mW with an absorbed pump power of 1.7 W, and a threshold absorbed power of 330 mW. In this case, the output laser had an average

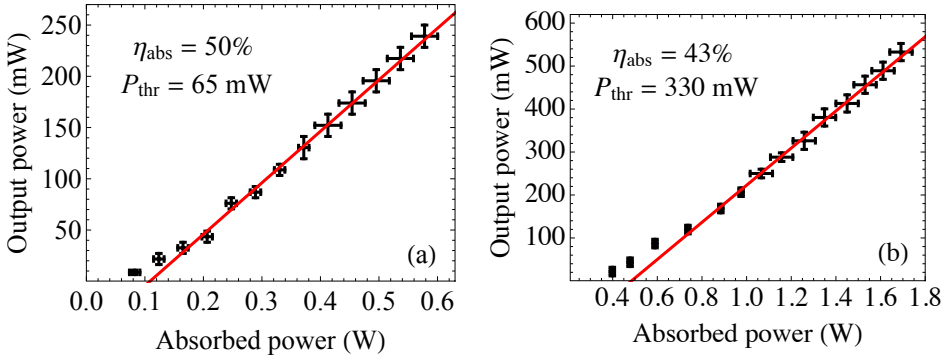

Fig. 6. Output power as a function of the absorbed pump power in free-running mode, when the Tm:SrF_2 crystal was pumped with the Ti:Sa laser (a) or with a diode laser (b). Slope efficiency (η_{abs}) and threshold absorbed power (P_{thr}) are also shown.

Optics EXPRESS

wavelength of about 2025 nm. Figure 6(b) shows the data measured with this setup. The slope efficiencies obtained under both pumping schemes are higher than the quantum defect of the laser $\lambda_p/\lambda_l \approx (787\text{nm}/2020\text{nm}) \approx 39\%$, confirming the presence of a resonant two-for-one pumping mechanism caused by the cross-relaxation between Tm ions.

By observing the emission cross-section, reported in Fig. 3, it is clear that those emissions were not purely electronic and were assisted by phonons. The laser did not oscillate at the peak of its gain because of the reflectivity spectrum of the mirrors employed in the resonators, which was centered around 2 μm. As expected, in the diode-pumping configuration the slope efficiency was lower and the threshold power was higher, due to the worse beam quality and larger spot size of the pump in the crystal, with respect to the one created by the Ti:Sa laser. Furthermore, the output power scaled well with the input power under diode pumping, showing no sign of thermal rollover.

Existing literature on solid-state lasers based on Tm-doped crystals includes several host materials in multiple resonator geometries. It should be noted that the slope efficiencies reported for lasers based on other host materials with similar output coupler transmissions do not significantly exceed our values, as illustrated in Table 1. We expect even better performance using an output coupler with higher transmission, which was not available during this work. In addition, the doping concentration in our Tm:SrF_2 crystal is lower than the one reported for laser operation in other Tm-doped laser materials (between 2 and 3 $\times 10^{21}$ ions/cm^3 in the respective lattices) [34, 41, 44].

The laser performance measured in this work supports the existence of a beneficial effect of clusterization on the cooperative processes that occur between close active ions in this material. However, there are other reports in literature of efficient Tm-based lasers with lower doping levels and concentrations, e.g. in sesquioxides [45]. Additional experiments on Tm:SrF_2 crystals doped with lower concentrations are required to further support this claim.

Table 1. Selected Results Reported for Laser Operation in Tm-Doped Single Crystals

Material	T_{OC}	η_{abs}	P_{thr} (mW)	P_{out} (mW)	λ_{out} (nm)	Ref.
Tm:$Gd_3Ga_5O_{12}$	0.8%	18%	390	580	2004	[46]
Tm:$(Lu–Gd)_3Ga_5O_{12}$	0.5%	20%	~200	170	~2015	[35]
Tm:$KLu(WO_4)_2$	0.5%	39%	820	1170	~2130	[36]
Tm:$NaGd(WO_4)_2$	0.4%	10%	430	330	1997	[47]
Tm:$LuVO_4$	0.5%	8%	160	450	1985	[48]
Tm:BaY_2F_8	0.5%	15%	120	162	1932	[44]
Tm:$LiLuF_4$	0.5%	56%	75	257	~2025	[34]
Tm:$GdLiF_4$	0.5%	53%	40	205	~2000	[41]
Tm:SrF_2	0.3%	50%	65	240	2015	This work
		43%	330	530	2025	

4.3. Wavelength tunability results

We investigated the spectral tunability of Tm:SrF_2 in the 3-mirror setup described before. During this measurement, the crystal was pumped with the Ti:Sa laser as described before, leading to an absorbed pump power of 0.9 W. By rotating the quartz birefringent plate, we selected the wavelength in which the laser was operating. This filter has a free spectral range of about 260 nm

Optics EXPRESS

around a wavelength of 2 μm and a linewidth of about 10 nm.

Figure 7 shows the output power escaping from the resonator as a function of the average wavelength of the radiation emitted. It can be seen that the laser was continuously tunable from 1840 nm to 2020 nm, exhibiting an uninterrupted tuning range of 180 nm. Operation at longer wavelengths was prevented by hopping on the other side of the tunability spectrum, caused by the birefringent filter curve and by the transmission of the mirrors employed in the resonator.

Spectral tunability of Tm-doped solid-state lasers has been reported so far in various materials. Results typically cover wavelength ranges between 1850 and 1950 nm for electronic transitions, extending up to 2050 nm for vibronic lasers [48, 49]. The broadest tunability ranges reported extend for about 210 nm e.g. in Tm:BaY_2F_8 or in Tm:Lu_2O_3 [44, 50]. The spectral tunability obtained in this work is thus comparable with existing sources.

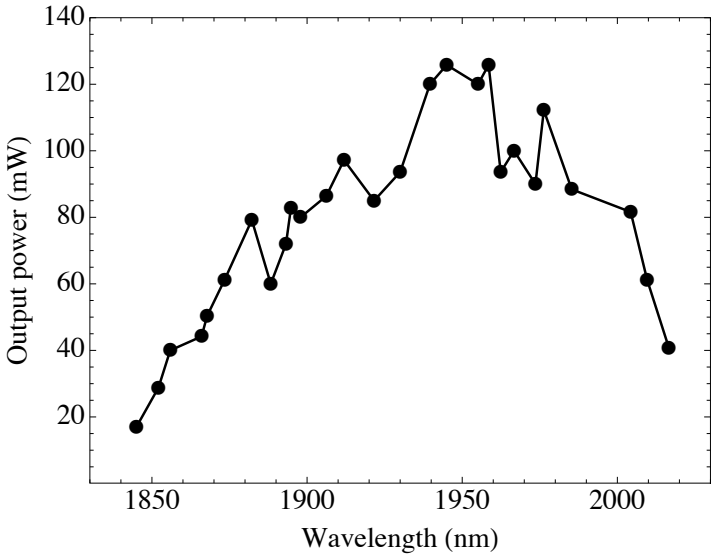

Fig. 7. Tunability curve of Tm:SrF_2 laser, measured at 0.9 W of absorbed pump power.

5. Conclusion and perspectives

We have reported on the first tunable continuous-wave laser operation of a 5.2 mol.% Tm^{3+}-doped SrF_2 single crystal. We investigated a low doping level of Tm ions, in comparison with the one typically embedded in other Tm-doped crystals [34, 41, 44], to investigate the effects of dopant clusterization in this material.

Elemental analyses evidenced a mild dopant segregation, as expected for small fractions of thulium, and determined the amount of dopant embedded in the crystal. Subsequent spectroscopic characterizations revealed the presence of broad absorption and emission bands, in contrast with other rare-earth-doped fluorides, confirming the presence of inequivalent doping sites. We evaluated the gain cross-section for this material, obtaining peak values that were comparable with earlier reports on this doping ion.

We obtained continuous-wave laser emission at about 2 μm by using two different pumping schemes. Using a Ti:Sa laser as pump source, we obtained a slope efficiency of 50% with respect to the absorbed pump power, and a maximum output power of 240 mW. Under diode-pumping excitation, we achieved a slope efficiency of 43% with respect to the absorbed pump power, with a maximum output power of 530 mW. Results obtained under laser diode excitation are particularly appealing for decreasing the complexity and sizes of a source based on this crystal.

Optics EXPRESS

These laser performances are comparable with existing literature on Tm-doped solid-state lasers, suggesting the presence of beneficial effects due to clustering on the cooperative mechanism between Tm ions. In addition, it should be possible to increase the slope efficiency of this crystal by employing output mirrors with higher transmittance, as usually done in other reports on these lasers. Furthermore, Tm:SrF_2 performed well also in comparison with its isomorph Tm:CaF_2, in which a slope efficiency of 32% was reported using an output transmittance of 2.6% [16].

We investigated the spectral tunability of this Tm:SrF_2 laser, obtaining an uninterrupted tuning range of 180 nm, extending from 1840 to 2020 nm. This wavelength range is on par with many other Tm-based tunable sources, but still under the span reported in some other crystals. Broader tunability at even longer wavelengths should be possible by optimizing the resonator setup and by employing higher pump powers. Unfortunately, tunability experiments performed using our diode laser as pump did not improve the tuning range, because of the much larger pump spot size in the active crystal.

Further work should be performed to optimize the laser performance of Tm:SrF_2, starting with increasing the output transmittance of the resonator and employing pumping sources with higher brightness and power. An investigation of the spectroscopic features and of the laser parameters as a function of the concentration of Tm ions should also be made, to quantify the clustering effects and, possibly, to reduce even further the doping level in the active medium. Finally, the laser results obtained in this work, combined with the clustering mechanism and the low phonon energy of SrF_2, encourage the exploration of doping with other rare-earth ions in this material.

Acknowledgments

The authors would like to thank Dr. C. Kränkel for helpful discussions about the experiment and I. Grassini for her expertise and assistance during the preparation of crystal samples.

Disclosures

The authors declare that there are no conflicts of interest related to this article.